Vision, Modeling, and Visualization (2010)

Geometric Reconstruction of the Ostium of Cerebral Aneurysms

Mathias Neugebauer†[1], Volker Diehl[2], Martin Skalej[3] and Bernhard Preim[1]

[1]Department of Simulation and Graphics, University of Magdeburg, Germany
[2]MR- and PET/CT-Center Bremen, Germany
[3]Department of Neuroradiology, University Hospital Magdeburg, Germany

Abstract

Polygonal 3D-reconstructions of cerebral aneurysms, combined with simulated or measured flow data provide important information for medical research, risk assessment and therapy planning. Landmarks, orientation axis, and a subdivision into functional unities, support the purposeful exploration of this complex data. The ostium, the area of inflow into the aneurysm, is the reference structure for various landmarks, axis and the initial subdivision into aneurysm's body and parent vessel. We present an approach to automatically extract important landmarks and geometrically reconstruct the ostium. Our method was successfully applied to various types of saccular aneurysms. These results were discussed with radiology experts. Our approach was considered as useful to reduce interpersonal variance in the ostium determination and forms a basis for subsequent quantification and exploration.

Categories and Subject Descriptors (according to ACM CCS): Computer Graphics [I.3.5]: Computational Geometry and Object Modeling—Computer Graphics [I.3.8]: Applications—

1. Introduction

A cerebral aneurysm is a pathological artery dilatation and forms an area with a high risk of rupture. The 3D-reconstruction of the affected vessel, often combined with flow data retrieved from CFD simulation or in-vivo measurements, provides the data basis for a broad range of medical applications: from research concerning the cause of aneurysm formation, over risk evaluation and stent planning, up to the development of new, minimal invasive treatment techniques.

Important information like maximum flow velocity or the mean wall shear stress can be retrieved without any functional decomposition of the 3D-reconstruction and the according flow field. This is suitable for initial risk estimation or a rough classification. Nevertheless, when it comes to specific tasks, like the detailed evaluation of local flow changes gained by a new stent design or an automatic geometry based comparison of several aneurysms, a subdivision of the given data into functional unities is often necessary. Since the flow characteristic is mainly influenced by the surrounding vascular geometry [TCS*10], the subdivision is performed based on landmarks retrieved from this geometry. The ostium, the

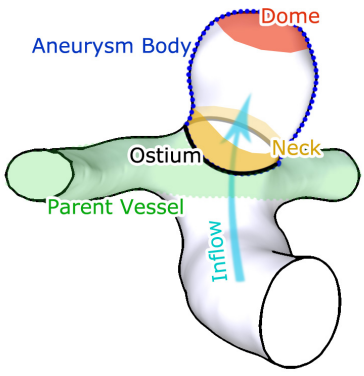

Figure 1: *Structural parts of a Saccular Aneurysm: The ostium seperates the aneurysm body from the parent vessel. The aneurysm body can be decomposed into neck and dome.*

† mathias.neugebauer@ovgu.de

DOI: 10.2312/PE/VMV/VMV10/307-314

area of inflow into the aneurysm (see Fig. 1), plays an important role in this process. Given a well-defined ostium, the aneurysm can be separated from the non-pathologic parent vessels. Based on this, the aneurysm's body can be decomposed into the dome and neck region. Several diameters and axes, like the central ostium-to-dome axis or the widest diameter within the aneurysm, can be calculated automatically. These geometric information is used to classify an aneurysm, support treatment decisions, adapt the visualization of the aneurysm and the flow field and support the interaction, when a medical expert explores the data.

To provide the basis for these applications, we present an approach for the detection of the ostium that takes the polygonal surface data, one manually selected point on the aneurysm surface and the centerline of the parent vessel as input. It provides the deformed ostium plane, the dome point, a central aneurysm axis and four control points and paths to support subsequent manual correction if necessary.

An initial requirement analysis (Sec. 4) was performed, concerning the geometric characteristics of the ostium and the medical workflow. The detection process (Sec. 5) is based on the analysis results and was evaluated with seven representative aneurysm datasets (Sec. 6). A subsequent discussion with radiology experts gave input for future applications (Sec. 7) that benefit from the extracted geometric information.

2. Related Work

A global analysis of intravascular hemodynamics, considering the complete flow field, provides useful data for the characterization of cerebral aneurysms. This includes parameters like grade of vorticity, maximum blood flow velocity [CCA*05] or the distribution of the wall shear stress [NGB*09], which are derived from computational fluid dynamics (CFD) [KBDL09]. Current medical research also involves a detailed analysis of specific functional parts of the aneurysm and the corresponding section of the flow field. Examples are the analysis of the stability of the pulsatile flow at the ostium of the aneurysm [MBHM09] or the relation between the risk of rupture and the inflow jet angle [BSH*10]. In both cases, a geometric description of the ostium is needed.

To detect and model the ostium, we need to enrich the undifferentiated geometric model of the aneurysm with axis, landmarks and other geometric descriptors. Such anatomical coordinate systems are common in medical diagnostics and treatment. Besides the purpose to support communication (e.g. *"a tumor in liver segment 6"*), they enable quantification and classification of anatomical structures, intervention planning or geometric modeling.

As an example, an automatically positioned mid-saggital plane is used to classify specific anatomic structures, like lymph nodes or tumors and separate them into left- and right-sided [RHD10]. Another example is the pre-operative planning for shoulder arthroplasty. This process involves a complex scapula coordinate system that is based on several landmarks and axes, which are derived from the patient specific bone geometry [KdBV*09]. An application for geometric modeling is discussed in [DWB*10]. They define local axes and geometric shapes based on landmarks derived from tissue slice images of the human eye, in order to generate a 3D-model.

Due to the tubular structure of vessels, systems for vessel reconstruction [VZB*05] and geometric analysis often involve the centerline as an abstract shape descriptor. The different approaches to obtain a centerline can be classified by method (thinning, distance transformation, Voronoi diagrams) or input data (continuous, discrete, polygonal). A comprehensive overview is given in [BFLCLC02].

Since polygonal surface data is available as input and to avoid sampling problems that occur when discrete distances (e.g. voxel size) are used, we apply a Voronoi diagram approach as described in [APB*08]. They present a framework, consisting of segmentation, reconstruction, geometric modeling and simulation. This framework was also applied to aneurysm datasets [PVS*09]. Among others, they quantify the angle between the parent artery bifurcation and the aneurysms neck plane. However, no detailed reconstruction of the ostium, based on the aneurysm's morphology, was performed.

In [KAB*04], an image-based approach for a more detailed definition of the ostium is presented. Their approach processes the individual image slices. After calculating the centerline points slice by slice, they map circles on the circular cuts through the parent vessel and determine the ostium area by means of radius analysis. This approach works well, as long as the parent vessel has an almost circular cross-section. As soon as it deviates from this shape, the ostium detection becomes inaccurate. However, due to pathologic changes of the vessel wall, the cross-section of the parent vessel often exhibits increased shape variance near to the aneurysm.

Therefore, instead of starting from within the parent vessel, our approach to determine the ostium is based on unique landmarks that can be defined on the aneurysms surface. A short description of the pipeline we apply to create the polygonal surface that serves as input data for our approach is given in the next section.

3. Input Data

The geometric information calculated by our approach shall support the characterization and exploration of simulation results. Since the simulation takes a polygonal aneurysm representation as input, we also derive the geometric information from this polygonal mesh.

The volumetric data, the polygonal mesh is derived from,

are MRA or CTA image slices with contrast enhanced vessels. Due to the good contrast, a basic segmentation, like thresholding combined with a Connected Component Analysis, is sufficient to extract the vessel from such dataset. Additionally, neurology experts analyze the anatomical plausibility of the segmentation results. Common problems are incorrect connections between adjacent vessels due to the partial volume effect and overly decreased vessel diameters close to the aneurysm due to beam hardening, caused by the high amount of contrast agent within the aneurysm. If necessary, the segmentation results are manually corrected.

An initial polygonal representation is created by applying Marching Cubes to the image data masked by the dilated segmentation mask. The triangle quality (aspect ratio, size gradient) of meshes derived from Marching Cubes is not sufficient, to form the basis for a simulation grid. Hence the mesh is rebuild by an advancing front algorithm and optimized by a combination of metric and topological changes (for details see [Sch97]).

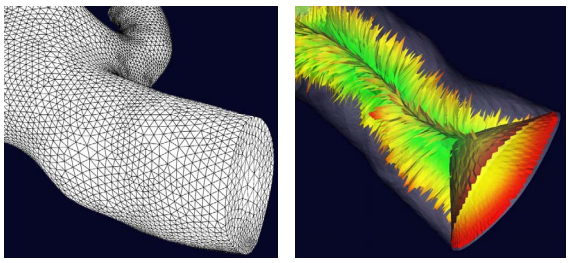

(a) Surface mesh (b) Polygonal representation of the Voronoi diagram

Figure 2: *The high quality surface mesh (2(a)) is the input for the centerline computation, based on the Voronoi diagram (2(b)).*

The centerline is derived from the polygonal model, utilizing its Voronoi diagram. A robust implementation is given as part of the Vascular Modeling Toolkit (VMTK), for details we refer to [APB*08]. The resulting centerline is represented as a polygonal line-strip. In combination with the high quality surface mesh it forms the input data for our geometric reconstruction approach (see Fig. 2).

4. Analysis of Geometry and Requirements

The ostium is the geometric feature of main interest, since it allows to separate the aneurysm from the parent vessels. It is also the starting point for further decomposition of the aneurysm and the definition of additional axis and feature points for measurement and interaction. We investigated the general medical definition of an ostium, how it is typically shaped and what landmarks can be used to describe this shape in a more abstract, geometric manner. We choose three representative polygonal aneurysm geometries from our database and asked six radiology experts, to describe the type, the characteristic shape, the frequency of occurrence of each aneurysm and the therapy they would select. Additionally, they were asked to draw the ostium on several different views of each aneurysm, if possible (see Fig. 3).

(a) Expert 1 (b) Expert 2 (c) Expert 3

Figure 3: *Extract of the survey results: drawings of three radiology experts on three different views of the same dataset.*

The results indicated that an ostium can only be defined for saccular aneurysms. This type of aneurysms has the highest frequency of occurrence (about 90% of all treated aneurysms). Fusiform aneurysms are an inhomogeneous dilatation over a certain length of the vessel and bear almost no distinct features. Additionally, they are often treated surgically. In that case, the exploration of flow data plays a minor role, in contrast to a minimally invasive therapy, where the flow is analyzed to estimate the success of a stent deployment. Thus, our geometric analysis approach is restricted to saccular aneurysms.

The geometric description (see Fig. 4) derived from the analysis of the ostium drawings indicated that the ostium plane is roughly bent around the centerline of the parent vessel. Two points on the parent vessel surface, before (P_1) and after (P_2) the bulging of the aneurysm, are always crossed by the contour of the ostium. The bending of the ostium plane can be described by two additional points (P_3, P_4). These points are orthogonally shifted away from the dome. $\vec{N}$ describes the orientation of the bent ostium plane and is perpendicular to the vector $\overline{P_1P_2}$. It points towards the dome point D. This point is defined as the surface point on the aneurysm that has the highest Euclidean Distance with respect to the parent vessel's centerline C. The contour also needs to provide a minimal distance between P_1, P_2, P_3, and P_4 with respect to their geodesic distance.

To summarize: the ostium can be described as a contour defined by four points. Two of them are located where the aneurysm emerges from the parent vessel and the other two describe how the ostium bends around the parent vessel. In order to model the ostium, we need to identify these abstract landmarks in a robust manner.

From qualitative interviews with the medical experts, we derived requirements that a system for geometric reconstruction must meet, in order to be usable in clinical workflows. Since the ostium is a supporting structure for subsequent quantification, interaction, and exploration, the effort

to model the ostium, with respect to computation time and interaction, needs to be low. Therefore, only a single, manually selected point, roughly placed on the aneurysm's body, is required as an initial hint for the detection of the above-mentioned landmarks. To avoid an interruption of the workflow, the time span necessary to generate the ostium should be in the scale of seconds. During this automatic process, information should be gathered that support an easy manual editing of the ostium shape afterwards. Thus, the clinician can continue his work, even in case the approach fails due to a very specific anatomical configuration or his personal interpretation of the ostium shape differs from the aforementioned abstract geometric description.

5. Ostium Modelling

There is more than one way to abstractly describe and subsequently reconstruct the ostium. We choose to rely on only a few feature points that, in case of correct or at least acceptable placement, enable us to reconstruct the complete ostium. Compared to surface and curvature based approaches (e.g. moving an active contour on the aneurysm surface in order to detect the ostium), our approach is quite robust, since it is less sensitive to local anatomical variations. Additionally, the intermediate results generated in some of the reconstruction steps can be useful as input data for manually editing the ostium plane afterwards. Our approach consists of the following steps: first we need to position the four control point P_1 - P_4, depending on the anatomical situation, then we create a contour that is smooth and minimizes the surface distance between the control points and finally build a mesh based on it.

5.1. Dome Point Estimation

The estimation of the dome point D takes the polygonal input data (parent vessel's centerline C, the surface mesh M), and the manually selected point P_M on the aneurysm body as input. For each vertex adjacent to P the distance to C is calculated. P is shifted to the position of the vertex with the highest distance. This process is repeated until no adjacent vertex has a shorter distance than P_M. In that case, the highest local distance to C is reached, which corresponds to the position of D (see Fig. 5). In case of smooth, satellite-free aneurysms, D correlates with the actual dome of the aneurysms. If satellites or comparable surface features are present, D can be placed at their local maximum distance to the centerline. Nevertheless, as long as D is positioned on the aneurysm surface and above the ostium, it is suitable for the following geometric construction steps.

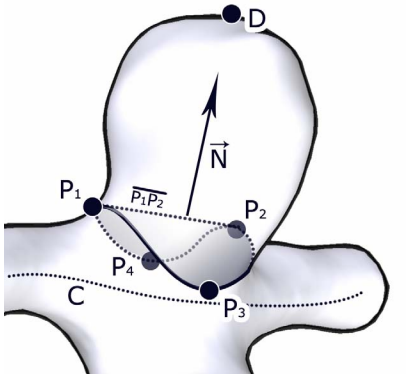

Figure 4: *Result of the geometric analysis of the expert's drawings.*

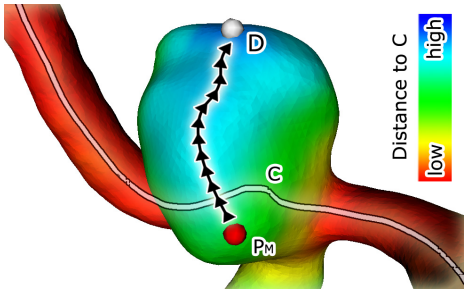

Figure 5: *Dome Point Estimation: M is moved iteratively, until the maximal local distance to C is reached.*

5.2. Restricting the Search Space for P_1 and P_2

The two landmarks P_1 and P_2 need to be placed on the parent vessel surface M, close to the bulging of the aneurysms body. Since a lot of positions fulfill this general requirement, we need to restrict the search space on the surface. Because P_1 and P_2 should be centered on the vessel surface, a projection of the centerline C on M is a suitable restriction. We orient the projection direction such that the projected C (C') crosses D. Thus we ensure that P_1 and P_2 will be centered on the vessel with respect to the aneurysm body. The projection direction is $\overline{SD}$, with S being a point on C that lies on an equidistant position between V_1 and V_2, using a geodesic distance metric. These two points are defined by the constraint that all C-vertices in-between have an unobstructed view towards D (see Fig. 6), which was tested by simple ray shooting.

5.3. Detection of P_1 and P_2

P_1 and P_2 are located on C', at the two transition zones from vessel to aneurysm, and vice versa. In order to find those transition zones, we need to distinguish between the parts of C' that lie on the vessel and those that lie on the aneurysm body. This is carried out by an peak analysis of the distance histogram, based on the minimal distances between the vertices of C' and C (see Fig. 7). Since the bulging of the ostium occurs in a relatively small area of the parent vessel, we can assume that the global histogram maximum includes

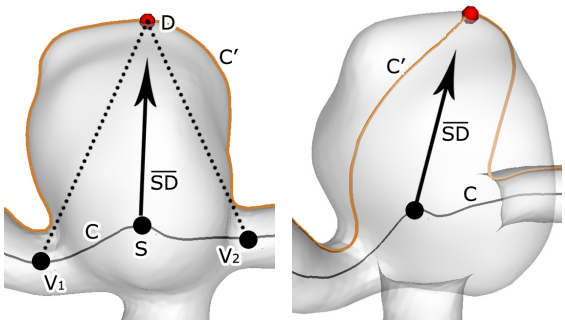

(a) Projection direction (b) Projected centerline

Figure 6: *The projection direction $\overline{SD}$ is constructed such, that the projected centerline C' is centered on the parent vessel with respect to the bulging of the aneurysm (6(b)).*

the mean vessel diameter D_V (more specifically half of the diameter, since we measure from the centerline). The vessel diameter near to an aneurysm tends to vary and can be slightly increased, due to vessel wall anomalies. Thus, we need to apply a scaling factor S_C, which is the only control parameter of our approach. Starting from the position of D on C', we iterate over the adjacent vertices in both possible directions and evaluate their distances to C. The first vertices "left" and "right" of the D with a distance $d \leq S_C \times D_V$ mark the position of P_1 and P_2.

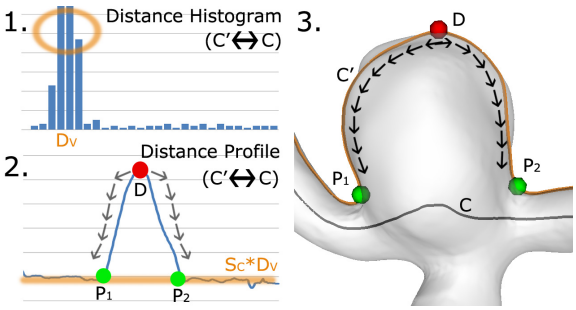

Figure 7: *The distance between C and C' is analyzed to find their mean distance D_V on the parent vessel. Using this distance, we find P_1 and P_2 by iterating over distance profile, beginning with the position closest to D.*

5.4. Building the Initial Ostium Contour

The initial ostium is the contour that results from cutting M with a plane that fulfills two requirements: the points P_1 and P_2 must lie within this plane and the plane normal must point towards Dt'(see Fig. 8). Hence, the normal-vector of the plane is perpendicular to the vector $\overline{P_1P_2}$. It can be described by a vector $\overline{AD}$, whereas A is the intersection point between $\overline{P_1P_2}$ and a plane that contains D and has $\overline{P_1P_2}$ as normal-vector. The resulting contour contains the points P_1 and P_2 and is positioned above the parent vessel, correctly oriented towards the aneurysm body. As control points for the subsequent bending of the ostium, we position two opposing points P_3 and P_4 at geodesically equidistant positions between P_1 and P_2 on the contour.

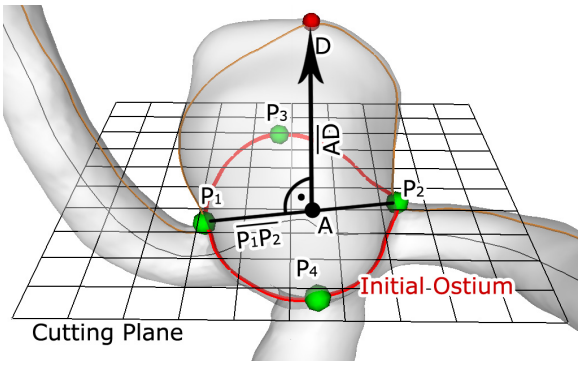

Figure 8: *The initial ostium is constructed by cutting the surface with a plane that has $\overline{AD}$ as normal vector.*

5.5. Bending the Ostium Contour

At the points P_1 and P_2 the ostium contour is already well placed. In order to complete the placement, we need to bend the contour near the points P_3 and P_4 towards the parent vessel. This is performed by shifting the points along paths that result from cutting M with planes that include D, comparable with the cutting the initial contour resulted from (see Fig. 9). The cutting planes are defined by D, a central ostium point B and P_1 (P_2 respectively), whereas $B = P_1 + 0.5 \times \overline{P_1P_2}$. P_1 and P_2 are shifted away from D along their corresponding paths until their distance to C is $d \leq S_C \times D_V$. Thus, the distance to all four control points (P_1 - P_4) corresponds to the mean parent vessel diameter. A Dijkstra algorithm is applied to compute geodesic paths between the control points and additional control points are placed halfway down these paths. The final ostium contour is represented by a closed spline-curve through all control points. Since we include geodesic paths, it is sensitive to local surface variations while enclosing the aneurysm bulging and resembling the transition zone from vessel surface to aneurysm.

5.6. Meshing the Ostium Plane

For various tasks, like calculating the aneurysms body volume or profiling the inflow through the ostium plane, it is necessary to have a surface representation of the ostium. We start with a naive meshing, by linearly connecting all points of the bent contour with point B and uniformly subdividing these connections (see Fig. 10).

Due to the linear meshing the original parent vessel shape

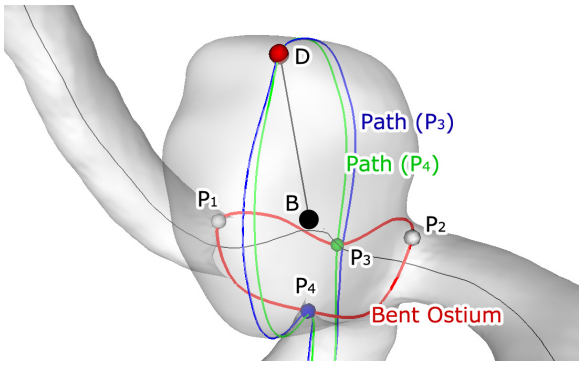

Figure 9: *The ostium is bent by shifting P_3 and P_4 away from D. The according paths are created by cutting planes.*

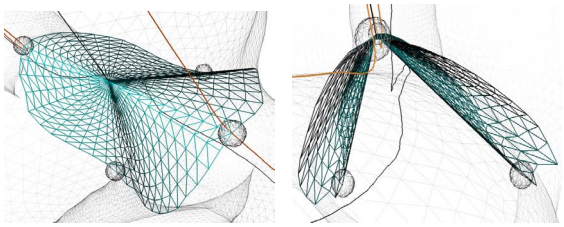

(a) View from above (b) View from side

Figure 10: *Due to the linear construction process, the initial mesh represents the original shape of the parent vessel poorly.*

is poorly approximated (see Fig. 10(b)). To improve this, we incorporate the distances of the contour- and saddle-points to a simplified centerline $\overline{P_1'P_2'}$ (see Fig. 11(a)), whereas P_1' and P_2' are the points on C with the closest proximity to P_1 and P_2. This simplification is necessary, since the centerline below the ostium tends to be bent into the aneurysm, which does not resemble the original vessel course.

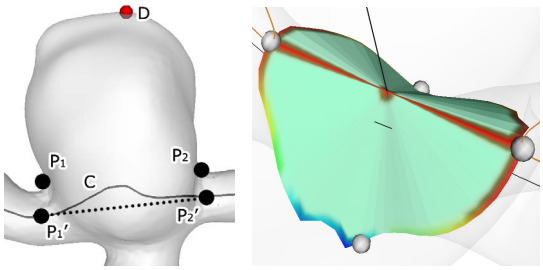

(a) Simple centerline $\overline{P_1'P_2'}$ (b) Distances for interpolation

Figure 11: *The original centerline bends into the aneurysm. As shown in 11(b), it can even pierce through the initial mesh. Thus, we apply a simplified centerline to calculate the distances and shifting vectors for the global interpolation.*

Dataset	# Δ	t_{Detect}(%)	t_{Mesh}(%)	$t_{Overall}$ (s)
An_01	61088	64	36	2.747
An_02	42370	62	38	2.052
An_03	66100	68	32	3.416
An_04	46280	70	30	2.473
An_05	34644	60	40	1.413
An_06	67466	63	37	3.050
An_07	39392	69	31	2.088

Table 1: *Computation time and polygonal complexity of our datasets.*

The distances are smoothly interpolated by applying a global Shepard Interpolation and all points, except the contour- and saddle-points, are shifted orthogonally away from $\overline{P_1'P_2'}$, according to their new interpolated distances. As a result, the ostium plane bends around the centerline and resembles the original vessel surface more realistically (see Fig. 12).

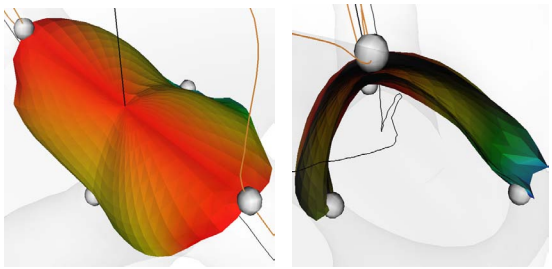

(a) View from above (b) View from side

Figure 12: *A global interpolation of the distances (comp. Fig. 11(b)) improves the shape of the ostium plane.*

6. Results and Evaluation

Our implementation is based on the Visualization Toolkit (VTK) and MeVisLab 2.0, which was used as prototyping environment. As input data, we used seven different polygonal models of saccular aneurysms that were derived from different imaging devices (CTA/MRA) during clinical standard procedures. Additionally, we used VMTK to calculate the centerlines of the parent vessel.

In Table 1 we present the polygonal complexity and computation time for each dataset and a percentage composition, showing the time portion spent for detection and for meshing. Although there is basic coherence between the number of triangles and the computation time, it can be observed that another parameter seems to influence the computation time.

For example, the datasets An_03 and An_06 have almost the same polygonal complexity, yet the dataset with the

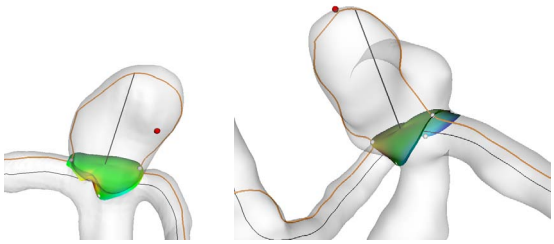

(a) An_06 (b) An_03

Figure 13: *Two datasets with aneurysms of different shape and complexity. The ostium plane adapts to local morphological features. The manual selected point is shown in red.*

slightly higher complexity has a significantly lower computation time. A visual comparison of both datasets (see Fig. 13) indicates that the dataset with the higher computation time also bears a bigger and more complex aneurysm body. This relation between computation time and aneurysm complexity holds for the other datasets as well. This is due to the local character of our approach. Even if some of the intermediate structures, like the projected centerline, are calculated for the whole dataset, most of the analysis is performed on or near to the aneurysm body. Our implementation is straight forward with no hardware acceleration or explicit focus on optimizing the computation time. Nevertheless, the computation time ranges from 1.4 to 3.4 seconds and is therefore already low enough for usage in a medical diagnosis workflow.

The ostium could be successfully reconstructed for all datasets, despite the variance in shape and parent vessel configuration. We used the ostium mesh to separate the aneurysm from the parent vessel (see Fig. 14) and presented the results to radiology experts. They interactively rotated the 3D-models and were asked to evaluate the quality of the separation. Except for one dataset, they stated that the cutting was plausible and correctly related to the particular morphologic situation. The dataset (An_07) that was not sufficiently separated was a rather rare case of an aneurysm with a very wide base (see Fig. 15).

The medical experts criticized the underestimation of the ostium as well as the shape of the ostium, which exhibited features that were not related to any surface feature. The continuous, almost feature-free transition from vessel to aneurysm was the main reason for the underestimation. Since the aneurysm was oriented almost parallel with respect to the parent vessel, the dome point detection was inaccurate which leads to an extreme orientation of the projected centerline. This finally resulted in a degenerated ostium plane, with three of the four control points forming a cluster on one side. This imbalance influenced the global interpolation and created the aforementioned waves.

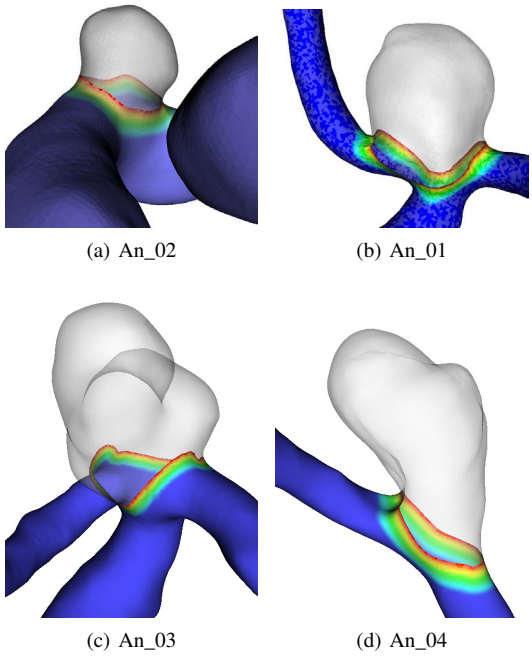

(a) An_02 (b) An_01

(c) An_03 (d) An_04

Figure 14: *A selection of the separation results: A broad variance in shape and complexity of the aneurysms and their parent vessel configurations can be observed. The distance to the cutting contour is color coded for visual clarification.*

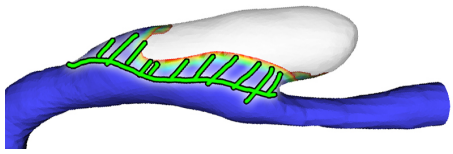

Figure 15: *The dataset An_07 contains a rare aneurysm type with a very wide neck and the aneurysm body being nearly parallel to the parent vessel. The underestimation of the ostium was marked by radiology experts.*

Even with all these inaccuracies, the ostium plane was oriented reasonably good. Geometric information (e.g. approximated ostium position and an initial central axis) could be derived from this plane and be used as input for a second pass. This additional information would improve the dome point detection process and the underestimated ostium contour could form the starting region for a specialized, surface-feature driven search for the real ostium contour.

While discussing these possibilities with the medical experts, it became clear that a fully automatic dectection process, which might handle all possible morphologic configurations, is not necessary. They wished for a system, which provides an initial ostium placement that can be easily ad-

justed if necessary. This is common in medical systems and enables the clinician to complete a process even in cases that are not covered by the automatic components of the system. Our approach provides the necessary prerequisites. The ostium can be completely adjusted by the four control points P_1 - P_4. Additionally, we provide control paths (see Sec.5.5) for a meaningful restriction of the degrees of freedom when moving the control points. Thus, our approach provides an initial, in most of the cases correct, placement of the ostium plane and delivers the needed structures for a subsequent manual adjustment.

7. Conclusion and Outlook

We described an approach to geometrically reconstruct the ostium of a saccular aneurysm. The reconstruction involves an iterative process that generates new geometric descriptors at each step. This process is based on the robust detection of specific landmarks whose abstract definitions were derived from an informal study with domain experts. The results showed that our approach is applicable to a broad range of morphological variations.

As a first application of the derived geometric information, we used the reconstructed ostium plane to separate the aneurysm from the parent vessel. The quality of the results was evaluated by radiology experts. Except for one, all separations were stated to be plausible. The exceptional case contained a rare morphologic configuration with a very wide neck and the aneurysm being almost parallel to its parent vessel. Nevertheless, even in that extreme case the ostium plane was oriented reasonable good.

Additional discussions with medical experts indicated that it should be possible to alter the geometrically reconstructed ostium in a subsequent manual step, either for correction or to adapt to unexpected requirements given by a specific medical workflow. Intermediate geometric information, created during the reconstruction process, can be used to support the interaction, e.g. by providing good views on the 3D-model or sensibly restricting degrees of freedom during interaction. We intend to develop interaction schemes and a workflow for this second, manual step.

As described initially, the basic motivation for our approach is to provide geometric data for various applications. This can be, but not exclusively, applications in the field of visualization (e.g. superimposing the ostium, different rendering for aneurysm and parent vessel, specific visualization of the inflow profile) or interaction (e.g. best view selection, supporting seed point placement for particle emitters, specific rotation and translation schemes during exploration).

Acknowledgment: We would like to thank U. Preim and her colleagues (University Hospital Magdeburg) for fruitful discussions and Fraunhofer MEVIS for providing the prototyping platform MeVisLab. This work has been funded by the federal state of Saxony-Anhalt in the scope of the MOBESTAN project (5161AD/0308M).

References

[APB*08] ANTIGA L., PICCINELLI M., BOTTI L., ENE-IORDACHE B., REMUZZI A., STEINMAN D.: An image-based modeling framework for patient-specific computational hemodynamics. *Medical and Biological Engineering and Computing 46*, 11 (2008), 1097–1112. 2, 3

[BFLCLC02] BÜHLER K., FELKEL P., LA CRUZ A., LA CRUZ R.: Geometric Methods for Vessel Visualization and Quantification-A Survey. *Geometric Modelling for Scientific Visualization* (2002), 399–420. 2

[BSH*10] BAHAROGLU M., SCHIRMER C., HOIT D., GAO B., MALEK A.: Aneurysm Inflow-Angle as a Discriminant for Rupture in Sidewall Cerebral Aneurysms. Morphometric and Computational Fluid Dynamic Analysis. *Stroke* (2010). 2

[CCA*05] CEBRAL J., CASTRO M., APPANABOYINA S., PUTMAN C., MILLAN D., FRANGI A.: Efficient pipeline for image-based patient-specific analysis of cerebral aneurysm hemodynamics: technique and sensitivity. *IEEE transactions on medical imaging 24*, 4 (2005), 457–467. 2

[DWB*10] DAI P., WANG B., BAO C., , JU Y.: Constructing a ComputerModel of the Human Eye Based on Tissue Slice Images. *International Journal of Biomedical Imaging 2010* (2010). 2

[KAB*04] KARMONIK C., ARAT A., BENNDORF G., AKPEK S., KLUCZNIK R., MAWAD M., STROTHER C.: A technique for improved quantitative characterization of intracranial aneurysms. *American Journal of Neuroradiology 25*, 7 (2004), 1158. 2

[KBDL09] KARMONIK C., BISMUTH J., DAVIES M., LUMSDEN A.: Computational fluid dynamics as a tool for visualizing hemodynamic flow patterns. *Methodist DeBakey cardiovascular journal 5*, 3 (2009), 26. 2

[KdBV*09] KREKEL P., DE BRUIN P., VALSTAR E., POST F., ROZING P., BOTHA C.: Evaluation of bone impingement prediction in pre-operative planning for shoulder arthroplasty. *Proceedings of the Institution of Mechanical Engineers, Part H: Journal of Engineering in Medicine 223*, 7 (2009), 813–822. 2

[MBHM09] MANTHA A., BENNDORF G., HERNANDEZ A., METCALFE R.: Stability of pulsatile blood flow at the ostium of cerebral aneurysms. *Journal of biomechanics 42*, 8 (2009), 1081–1087. 2

[NGB*09] NEUGEBAUER M., GASTEIGER R., BEUING O., DIEHL V., SKALEJ M., PREIM B.: Map Displays for the Analysis of Scalar Data on Cerebral Aneurysm Surfaces. In *Computer Graphics Forum (EuroVis)* (Berlin, 10.-12. Juni 2009), vol. 28 (3), pp. 895–902. 2

[PVS*09] PICCINELLI M., VENEZIANI A., STEINMAN D., REMUZZI A., ANTIGA L.: A framework for geometric analysis of vascular structures: applications to cerebral aneurysms. *IEEE Trans Med Imaging* (2009). 2

[RHD10] RÖSSLING I., HAHN P., DORNHEIM L.: Schätzung der Midsagittalebene zur Bestimmung der Seitenlage maligner Strukturen des Halses. In *Bildverarbeitung für die Medizin (BVM)* (2010), pp. 395–399. 2

[Sch97] SCHÖBERL J.: NETGEN An advancing front 2D/3D-mesh generator based on abstract rules. *Computing and visualization in science 1*, 1 (1997), 41–52. 3

[TCS*10] TATESHIMA S., CHIEN A., SAYRE J., CEBRAL J., VINUELA F.: The effect of aneurysm geometry on the intra-aneurysmal flow condition. *Neuroradiology ePub* (2010). 1

[VZB*05] VOLKAU I., ZHENG W., BAIMOURATOV R., AZIZ A., NOWINSKI W.: Geometric modeling of the human normal cerebral arterial system. *IEEE transactions on medical imaging 24*, 4 (2005), 529–539. 2